

Research paper

Modeling heart flow dynamics using numerical simulations to identify the vortex ring: A practical guide



E. Lazpita^{a,*}, A. Mares^c, P. Quintero^c, J. Garicano-Mena^{a,b}, S. Le Clainche^{a,b}

^a ETSI Aeronáutica y del Espacio - Universidad Politécnica de Madrid, 28040 Madrid, Spain

^b Center for Computational Simulation (CCS), 28660 Boadilla del Monte, Spain

^c ETSI Aeroespacial y Diseño Industrial - Universitat Politècnica de València, 46022 Valencia, Spain

ARTICLE INFO

Dataset link: [Simulation Codes \(Original data\)](#)

Keywords:

Computational fluid mechanics

Cardiac flow

Left ventricle model

ABSTRACT

In this study, we present a comprehensive numerical analysis of blood flow within human left ventricle models, with particular emphasis on optimizing simulation conditions to enhance the realism and computational efficiency of heart flow dynamics. The objective is to determine the most effective mesh configurations, flow conditions, and boundary settings necessary for accurately capturing the formation and behavior of the vortex ring—a pivotal element in ventricular flow dynamics. Utilizing a computational fluid mechanics approach, we review the influence of both idealized and patient-specific geometries on simulation outcomes. It is imperative to consider the necessity of dynamic wall motion and the precise calibration of inlet and outlet boundary conditions, which must be designed to mimic physiological conditions as accurately as possible. These factors are of paramount importance in achieving a balance between computational resource demands and the fidelity of the simulations, thereby providing valuable insights for future cardiovascular modeling efforts. Tutorials explaining details of the simulations and the codes used are included in ModelFLOWS-app website [14].

1. Introduction

Despite considerable advances in cardiovascular medicine, cardiovascular disease (CVD) remains the leading cause of mortality worldwide [1]. This has motivated extensive research into innovative diagnostic and therapeutic strategies. The accurate detection and analysis of cardiac flow dynamics are fundamental to the advancement of cardiovascular medicine.

Computational fluid dynamics (CFD) has emerged as a valuable tool for simulating cardiovascular flows. It offers a range of approaches and methodologies for modeling and analyzing the complex dynamics of blood flow within the heart. For instance, the open-source lifex-cfd solver demonstrates its utility in modeling blood flow under diverse physiological and pathological conditions. The study by Africa et al. [2] underscores the solver's precision and dependability in simulations conducted through the incompressible Navier-Stokes equations. Another study presents a novel left ventricular simulator that employs computational modeling to test cardiovascular implants. This simulator has the potential to serve as a low-cost and efficient testing platform for preclinical evaluations [3]. A comparative study of blood flow simulations using smoothed particle hydrodynamics (SPH) and finite volume

method (FVM) methods has been conducted, and the findings indicate that while SPH provides detailed insights, it is more computationally demanding [4]. Additionally, Zingaro et al. [5] show the integration of electromechanics and fluid dynamics to achieve a realistic blood flow simulation in a left ventricle (LV) model. A study combining statistical shape modeling with CFD using cardiac computed tomography (CCT) data has been carried out to explore intracardiac flow features as early predictors of heart diseases [6]. Finally, Thiel et al. [7] introduce IP-HEART, an open-source computational pipeline for processing patient-specific ventricular geometries derived from 3D echocardiography data. This approach addresses reproducibility challenges in CFD modeling and demonstrates the effectiveness of the method in simulating clinically relevant blood flow features.

Despite its potential, CFD faces challenges in the accuracy and reliability when applied in cardiovascular research and eventually, in medical practice. While it is increasingly used to model heart flow dynamics, there is a lack of comprehensive guidelines for fine-tuning simulations to ensure optimal performance and credibility. This study addresses these challenges by introducing a systematic approach to configure Star-CCM+ [8] simulations, a commercial solver used in the literature for

* Corresponding author.

E-mail address: e.lazpita@upm.es (E. Lazpita).

heart flow dynamics [9]. It places particular emphasis on accurately capturing the vortex ring, a critical flow feature in the left ventricle blood flow throughout the cardiac cycle.

The vortex ring is formed in the mitral valve of the left ventricle due to the jet entering through the orifice between the mitral valve leaflets. Initially, this vortex is planar, but as it enters an asymmetric cavity, it propagates and while doing so, experiences asymmetric growth and tilting during diastole. This is necessary to efficiently fill the ventricle chamber's elongated shape. This tilting is clockwise, with the left side remaining in the upper part due to the interaction of the ring with the ventricular walls, and the right side diving into the apex. This asymmetric development is crucial for efficient ventricular function, preventing stagnant areas and ensuring complete filling of the ventricle [10]. An understanding of this relationship between ventricular shape, motion, and vortex evolution is essential for comprehending overall ventricular function [11].

It has been demonstrated that variations in vortex ring formation and evolution can be linked to cardiovascular diseases. For instance, Mangual et al. [12] conducted a comparative evaluation of intraventricular fluid dynamics between healthy subjects and patients with dilated cardiomyopathy (DCM), identifying distinct differences in the vortical structures within the left ventricle. Similarly, Riva et al. [13] used 3D magnetic resonance imaging (MRI) data to highlight differences in the characteristics of the vortex ring, such as circularity, orientation, and inclination, between healthy hearts and those with ischemic cardiomyopathy (ICM).

The present study introduces a novel framework that improves the reliability and replicability of heart flow simulations. This development addresses a significant gap in the existing literature, wherein the available models frequently prove insufficient for accurately simulating complex cardiovascular dynamics with the desired level of replicability. This paper represents a significant advancement beyond a mere review of the literature. It effectively synthesizes the latest theoretical knowledge with practical applications. Consequently, our contribution represents a significant advancement over existing studies, offering unique insights and comprehension of the implementation selection, thereby facilitating more accurate and reproducible simulations. Furthermore, this article is enhanced by a practical guide, which can be found in Ref. [14], which shows the optimal methodology for configuring CFD simulations, with a particular emphasis on the most intricate aspects of mesh generation and boundary condition settings. To the best of the authors' knowledge, there are currently no articles in the literature that provide researchers with a clear and comprehensive approach to addressing this issue. This will facilitate the exploration of new research avenues and the resolution of emerging problems.

The article is organized as follows: Section 2 details the methodology employed in tuning the simulations, presents the results for various conditions, and discusses their implications. Section 3 demonstrates the validation process using an alternative code implemented in Ansys Fluent [15], as thoroughly explained in Ref. [16]. Finally, Section 4 summarizes the main conclusions of this work.

2. Simulation setup

In this section, we explore various conditions essential for optimizing our CFD simulations. The focus is on four key aspects: geometry of the model, flow modeling, mesh, and boundary conditions. Each of these factors plays a crucial role in the accuracy and efficiency when performing the simulations, particularly in their capacity to capture the vortex ring. This vortex is a pivotal indicator of efficient heart flow dynamics and requires precise simulation conditions to be depicted accurately. Our goal is to identify the simplest and most efficient methods for configuring these conditions, ensuring that they collectively contribute to a robust and reliable representation of the vortex ring in our simulations.

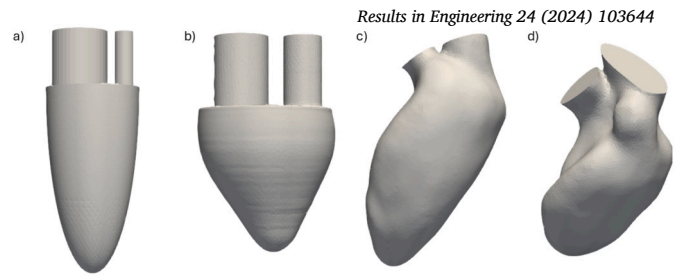


Fig. 1. Left ventricle models, increasingly more realistic from left to right. Extracted from reference: a) Zheng et al. [17] and b) Vedula et al. [18]. Patient specific models extracted from medical data: c) Patient 1 and d) Patient 2.

2.1. Geometry

Geometry plays a critical role in the accuracy of our results when performing the simulations. In this manuscript, we have focused on an idealized geometry in order to obtain a simulation of the blood inside the left ventricle that captures the vortex ring feature, and discuss the physics behind this phenomenon. Future research could consider modifying the idealized geometry and/or boundary conditions in order to simulate various forms of cardiovascular disease and examine the resulting changes to the flow patterns. This would enhance the potential relevance of the findings for clinical practice and personalized diagnostics. However, in order to facilitate a more generalized approach and to accommodate more complex geometries, we have also considered patient-specific left ventricle geometries in our tutorials.

Idealized geometries were constructed based on Ref. [17,18], while patient-specific geometries were derived from medical imaging data. The first patient specific geometry was extracted from medical data available online as open source in <https://figshare.com/s/2a5de3a2b89a3fb87932> with its accompanying article [19]. The second patient data was obtained through a collaboration with the *Centro Nacional de Investigaciones Cardiovasculares* (CNIC) [20] through the *DigitHEART* project [14]. This different models are depicted in Fig. 1.

Patient-specific geometries, when correctly represented, can provide more realistic and physiologically accurate results. However, these geometries also present several challenges. Obtaining these models is challenging due to the necessity of sophisticated medical imaging tools to create accurate CAD models of sufficient spatial resolution. Despite the availability of these tools, the segmentation and meshing process remains a significant challenge, both in terms of difficulty and automation. Additionally, the temporal resolution achieved during a heart cycle is often inadequate for the computational needs of our simulations, necessitating interpolation or other strategies to fill in data gaps. As a result, the person-cost of representing geometry and creating a mesh, along with the computational cost and complexity of the simulations, are increased.

Conversely, idealized models, while potentially oversimplified, can be useful for capturing the most critical features of heart flow dynamics in a more controlled manner with reduced computational demand. These models are easier to validate due to their comparability and simplicity. Furthermore, idealized models facilitate the incorporation of various heart pathologies by directly modifying the model, avoiding the need to find a patient with the specific condition or to extensively alter a patient-derived model. This simplicity makes idealized geometries an attractive option for simulations where control and cost are significant considerations. Therefore, for the sake of brevity, through the following discussion we will mainly focus on the idealized geometry extracted from Zheng et al. [17] selected from references for its simplicity when configuring our simulation.

We represent this model of the left ventricular cavity as a semi-ellipsoid with two cylindrical tubes attached in the top plane, which model the mitral and aortic valves. To accurately model the blood flow within a human left ventricle, it is essential to select the appropriate ge-

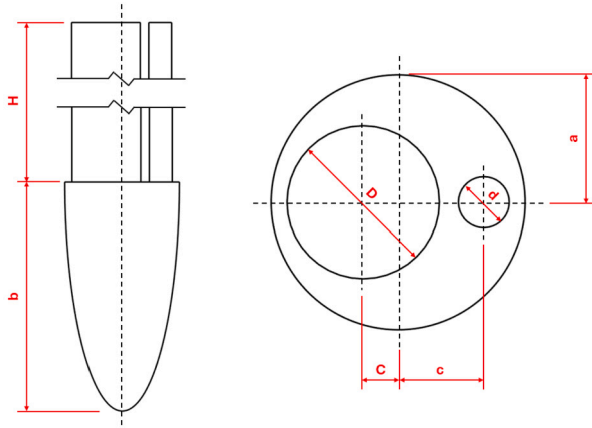


Fig. 2. Ideal geometry of the LV model extracted from Zheng [17].

ometrical parameters, ensuring a consistent end-systolic volume (ESV) for the LV model, which represents the minimum volume of the LV during a cycle. These include the semiaxis lengths ($a = 2\text{cm}$ and $b = 8\text{cm}$), the tube diameters ($D = 2.4\text{cm}$ and $d = 0.8\text{cm}$ for the inlet and the outlet, respectively), the height of the tubes (H), and finally, the distance between the centers of the tubes and the axis of the semi-ellipsoid ($C = 0.55\text{cm}$ and $c = 1.35\text{cm}$ for the inlet and outlet, respectively). Fig. 2 details further the geometry and the location of each geometrical parameter necessary to construct the model. With these dimensions, the volume in the ESV state for this model, without taking into account the tubes, can be calculated using the volume equation for a semi-ellipsoid with a circular base:

$$ESV = \frac{2}{3} \cdot \pi \cdot a^2 \cdot b = 67\text{ml} \quad (1)$$

The values of the dimensions, and consequently, the volume, are selected to match physiological values. The evolution of the volume of this geometry from ESV to end diastolic volume (EDV) and back is performed moving the outer wall of the semi-ellipsoid, which is further explained in Section 2.4.1.

2.2. Flow modeling

Selecting appropriate fluid conditions is of paramount importance for the accurate simulation setup. In our study, we model blood as an incompressible Newtonian fluid (based on Ref. [21,22]) with a constant density ($\rho = 1060\text{ kg/m}^3$) and dynamic viscosity ($\mu = 0.004\text{ Pa}\cdot\text{s}$). The Reynolds number can be inferred from these values by taking the inlet tube diameter, D , as the characteristic length and the maximum inlet velocity of the entire cardiac cycle ($V_{max} = 0.86\text{m/s}$) as the characteristic velocity. This will be discussed in greater detail in Section 2.4.2. Consequently, the Reynolds number can be defined as:

$$\text{Re} = \frac{\rho V_{max} D}{\mu} \simeq 5500 \quad (2)$$

Another typical non-dimensional parameter employed in cardiovascular simulations is the Womersley number, α , which quantifies the ratio of transient inertial forces to viscous forces and characterizes the pulsatile nature of blood flow. The Womersley number is defined as:

$$\alpha = D \left(\frac{\omega \rho}{\mu} \right)^{1/2} \simeq 31 \quad (3)$$

where ω is the angular frequency of the heart cycle which in our case is 2π . This value is greater than that observed in Ref. [23], since the characteristic length is approximately ten times larger.

In light of the findings presented in the literature, namely those of He et al. [24] and Tagliabue et al. [25], it is possible to accurately and

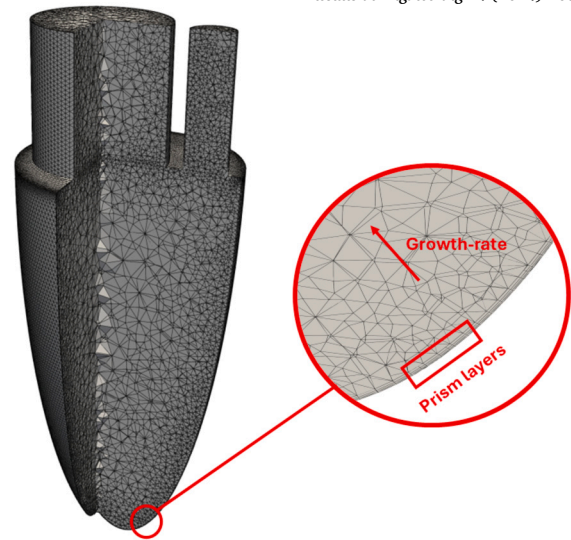


Fig. 3. Illustration of the mesh for the properties detailed in Table 1 and a base size of $7.5 \cdot 10^{-4}\text{m}$.

efficiently capture the formation and evolution of the vortex ring, a phenomenon that emerges in early diastole with low velocity, by assuming that the flow behaves as laminar and not considering turbulence in the simulations. Therefore, as our objective is to capture the vortex ring, in our study the blood flow is modeled as laminar.

However, given that the blood flow within the LV chambers is characterized by a regime of transition to turbulence, it is essential to include turbulence models in a detailed simulation that captures a wider range of scales and phenomena. Consequently, certain studies, such as those conducted by those by Bucelli et al. [26] and Korte et al. [27], employ turbulence models (Variational Multiscale - Large Eddy Simulation and Shear Stress Transport $k - \omega$ model, respectively) to capture the entirety of the features that manifest throughout the cardiac cycle, thereby facilitating the generation of highly precise simulations.

It should be clarified, however, that the present study is exclusively conducted using the laminar approach. The justification for this choice is provided in Sec. 3, where it is demonstrated that the formation and evolution of the vortex ring can be accurately captured.

2.3. Mesh

The process of meshing plays a pivotal role in our simulations, particularly in light of the intricate dynamics of fluid flow within a cardiac chamber. In these confined spaces, we encounter a multitude of small-scale phenomena that necessitate the use of a highly refined mesh to accurately capture the relevant flow dynamics.

To create our meshes, we changed some properties in the Star-CCM+ meshing tool, which are described in Table 1. First of all, we need to declare a base size which will be the default size of an element in our mesh. This size will vary over the volume depending on other properties such as the growth rate. In our study, we selected a $20 \cdot 10^{-4}\text{m}$ size to start with and then, in order to achieve mesh convergence, the base element size was decreased to obtain finer meshes. We then implement a mesh refinement approach that includes two primary strategies: applying a tetrahedral mesh to most of the domain at a given volumetric growth rate, ensuring that the mesh becomes increasingly refined as it approaches the walls, and incorporating four to six prismatic layers attached to the walls. These prism layers are particularly effective at adapting the mesh to the contours and movements of the walls, thus increasing the accuracy of our simulations. An auto-generative iterative process was employed in order to obtain a conformed and high-quality mesh. To facilitate a more comprehensive understanding of the mesh

Table 1

Mesh properties in the Star-CCM+ meshing tool. The base size reflects the standard size of the elements in our mesh, the volume growth rate specifies the rate at which the element size grows as we separate from the outer surface, the number of prism layers selects how many prism layers the user wants to add around the surface, and again the growth rate specifies the rate at which they grow.

Property	Value
Type	Hybrid Tetrahedral/Prism
Base size [m]	[20, 10, 7.5, 5] · 10 ⁻⁴
Volume growth rate	1.3
N° prism layers	5
Prism layers growth rate	1.2

and its associated properties, the volumetric mesh is presented in Fig. 3 at a medium resolution with a base size of $7.5 \cdot 10^{-4} m$.

It should be noted that the meshing process is not typically depicted in the literature, as it is a complex procedure when attempting to reproduce the findings of another study. This is because it necessitates a profound understanding and expertise with the solver. In Ref. [14], we present the methodology employed to tune our meshes.

This meticulous approach to mesh configuration is essential for capturing relevant phenomena at the wall boundaries, and also paves the way for the integration of wall motion and mesh transformation techniques discussed in the next section.

2.4. Boundary conditions

In our study, which focuses on an idealized LV model, we consider three primary boundaries: the ventricular wall, which can include its displacement; the inlet, which simulates the blood flow entering through the mitral valve; and the outlet, which represents the flow exiting through the aortic valve. Each boundary plays a pivotal role in accurately representing the physiological processes of the heart, thus necessitating precise definition to ensure the realism and success of our simulations.

As will be discussed in greater detail later on, our study employed a temporal profile for the ventricular volumetric flow rate, which was extracted from the source cited as Ref. [17]. The data presented here are measurements taken from an experimental setup of a ventricular model that is designed to mimic the ideal model. Nevertheless, current clinical practice, including 4D flow MRI, allows for the acquisition of precise, real-time measurements of blood entering or exiting the ventricular cavity. This may enhance the quality of the obtained results and facilitate more robust and accurate CFD simulations [28].

2.4.1. Wall

In the study of left ventricle hemodynamics, the selection of wall boundary conditions is a matter of careful consideration. The decision to employ fixed walls or periodically moving walls, which more closely reflect the dynamic nature of the heart, is of critical importance, yet it introduces varying degrees of complexity to the implementation and analysis. At first, the walls were considered fixed throughout the cardiac cycle with the objective of approximating inflow and outflow rates to match idealized or physiological data. However, our initial experiments demonstrated that fixed walls were unable to accurately model the flow dynamics within the ventricle; key features such as the vortex ring or recirculation to the apex were not captured. This highlights the limitations of the fixed wall configuration in representing the intricate flow patterns within the ventricular chamber.

In light of the critical importance of capturing accurate dynamics, we turned to an implementation of moving walls. However, this posed significant challenges. Fig. 4 illustrates a schematic approach of the methodology used to obtain the wall movement, showing the volume

flow rate and volume change graphs in the top row and some time instants of the evolution of the mesh during a cardiac cycle.

In this study, we employed flow rate data extracted from Zheng et al. [17], which represents the volume of blood entering the left ventricular chamber per unit of time during a heart cycle. In our approach, the heart rate was assumed to be 60 beats per minute, so the heart period was $T = 1 s$. From now on, time will be normalized to the period as $t^* = t/T$ for generalization purposes. Given the assumption of incompressibility for the blood flow, integration of the flow rate data allows the determination of the volume change of the LV model for each time instant. To this end, the raw flow rate data extracted from the reference was first interpolated into a temporally equispaced grid using the “interp1” function with the “spline” method. The spline method was selected due to its well-documented accuracy and smoothness which makes it a popular choice in fluid dynamics simulations [29,30]. Subsequently, the integral was calculated using the “integrate” function, which employs a numerical integration method. The aforementioned process and methodologies were implemented in Matlab [31] and are illustrated in the upper panel of Fig. 4.

Once the evolution of ventricular volume $V(t^*)$ has been calculated, the long and short semiaxis values for each time instant can be calculated using the semi-ellipsoid volume equation and maintaining the 4 to 1 ratio ($k = 4$) between $b(t^*)$ and $a(t^*)$:

$$b(t^*) = \left[\frac{3}{2\pi} \cdot k^2 \cdot V(t^*) \right]^{1/3} \quad (4)$$

$$a(t^*) = k \cdot b(t^*) \quad (5)$$

The geometry was initially constructed as the minimum volume of the ventricle, the end-systolic volume (ESV), at time $t^* = 0$. It then undergoes a uniform expansion following the previous equations to attain the maximum volume, the end-diastolic volume (EDV), at time $t^* = 0.67$, before reverting to the ESV at time $t^* = 1$. This is illustrated in the bottom of Fig. 4.

By obtaining the volume change and defining the geometry for each time instant, we have gathered the required data for the implementation of the wall movement. The data will be utilized by each solver or tool in a manner contingent upon the implementation of the code.

For our study employing Star-CCM+, it is initially essential to normalize the volume variation between 0 (ESV) and 1 (EDV) to employ the data in the “morphing” tool as incremental displacements. Subsequently, utilizing the “diff” function of Matlab, the displacement of the mesh was calculated in order to align with these changes, effectively morphing it to adapt to the dynamic volume alterations.

The comprehensive manipulation of this data has facilitated the implementation of the wall movement in Star-CCM+. The initial step is to construct or import the model in its minimum volume instant. Subsequently, the model must be defined in its maximum volume state and the total displacement from the minimum to the maximum volumes must be extracted from the mesh states obtained earlier. Finally, the incremental displacements between each time step must be introduced as a morphing wall boundary condition to guide the morphing process for the volume changes to match the flow rate graph.

This implementation enabled the simulation of ventricular wall movement in a manner that approximates the physiological reality. The simulation successfully captured key features, such as the vortex ring and other essential characteristics of cardiac flow within the ventricle.

However, other solvers, such as Ansys Fluent, require an alternative approach to wall movement. For this implementation, the evolution of the volume at each time instant must be provided as STL files. Subsequently, a Python script is used to convert these files into data that Fluent can read as a mesh with user-defined functions. Finally, each mesh file is loaded and the wall location is defined at each time instant.

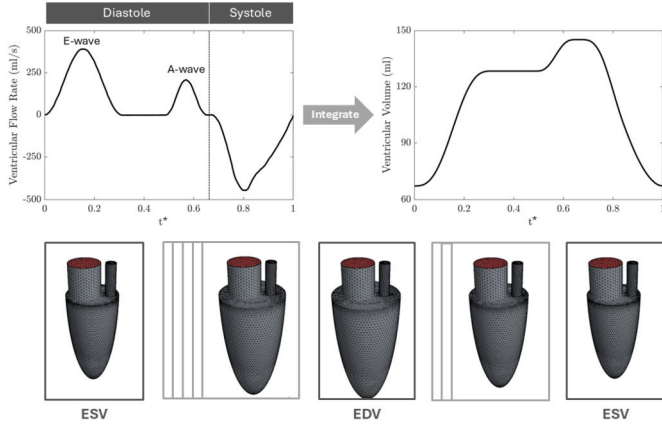


Fig. 4. (Top) A detailed plot of the volumetric flow rate of the LV model during a heart cycle, extracted from Ref. [17] and the volume variation graph of the same model obtained via integration in Matlab are provided herewith. (Bottom) Representation of the various mesh states from end-systolic volume (ESV) at time point zero to end-diastolic volume (EDV) at time point 0.67 and back to ESV at time point one.

2.4.2. Inlet

The selection of appropriate inlet boundary conditions is of critical importance, particularly in the context of modeling the flow entering the idealized LV model. Our objective is to accurately reproduce the dynamics of this flow, taking into account a number of factors, including the length of the inlet tube, the type of boundary, and the temporal and spatial distribution of the incoming flow.

Our initial experiments explored different boundary condition types, such as pressure inlet, velocity inlet, and mass flow inlet. A pressure-only boundary condition was initially employed, which permitted the flow to proceed inside the ventricle due to the pressure gradients created by ventricular expansion. In our experiments with this boundary condition, we observed suboptimal performance in capturing the relevant flow patterns and encountered difficulties in modeling the mechanical actions of the mitral valve (opening and closing), which are essential for accurate modeling of intracardiac flows.

In contrast, the utilization of either a velocity or mass flow inlet proved more effective in our study in accurately capturing the valve closure and overall flow dynamics. However, the performance of these approaches is contingent upon the precise definition of the flow profile, both temporally and spatially. In terms of temporal characteristics, the flow profile must closely resemble the physiological data, exhibiting a large peak corresponding to the E-wave, followed by a smaller peak for the A-wave, and ceasing during valve closure. This information was extracted from the flow rate graph in Fig. 4 and modified for zero flow/velocity in systole.

In regard to the spatial distribution of the profile, the most common initial choice is the plug profile, which employs a uniform distribution. However, due to the presence of a wall-bounded tube, a discontinuity in the flow may occur in the immediate vicinity of the wall, where both zero velocity (no-slip wall boundary condition) and a velocity profile are imposed. Accordingly, we have also included profiles that may mitigate this discontinuity, such as a parabolic profile or a midway approach as the hyperbolic tangent, wherein the velocity in the wall is set to zero and then grows to a value approaching that of the plug profile for the tube center. In all cases, the flow rate was maintained constant, with the necessary corrections being introduced in the equations. Consequently, our study will encompass three distinct spatial profiles, as illustrated in Fig. 5:

$$V_{plug} = V(t^*) \quad (6)$$

$$V_{parabolic} = \left[1 - \left(\frac{r}{R} \right)^2 \right] V(t^*) \quad (7)$$

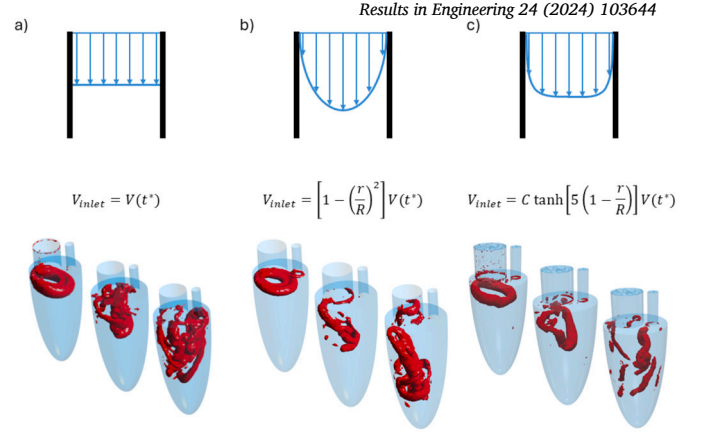


Fig. 5. Each column represents a different inlet spatial profile: a) Plug; b) Parabolic; c) Hyperbolic tangent. (Top) Schematic representation of the inlet profile in a 2-d section. (Center) Equation for the velocity inlet spatial profile. (Bottom) Q-criterion isosurfaces for $t^* = 0.16, 0.26, 0.40$ from left to right, depicting the evolution of the vortex ring.

$$V_{tanh} = C \cdot \tanh \left[5 \left(1 - \frac{r}{R} \right) \right] V(t^*) \quad (8)$$

where C is the constant used to match the flow rates.

The hyperbolic tangent distribution was found to be the most effective, demonstrating improved convergence on coarser meshes and reduced computational cost while accurately capturing the main dynamics of the vortex ring. These dynamics include the formation of the circular ring in early diastole, a clockwise tilt due to the proximity of the wall on one side of the ring, and the reduction of the inflow velocity. Additionally, the instability growth and final dissipation of the ring at the end of diastole were accurately represented. The plug profile also captured the main dynamics just mentioned, but proved to be more computationally demanding, requiring finer meshes to achieve convergence. Finally, the parabolic profile proved to perturb the incoming flow excessively, causing the ring to reach too deep, thus slowing down the tilt, enlarging the structure and making the growth and dissipation of the instability slower and later in the cycle, thus affecting the overall flow dynamics. In Fig. 5 we can see these results illustrated, showing the schematic of the different inlet profiles just at the beginning of the inlet tube in a 2-d section at the top, the equation in the middle and three different time instants ($t^* = 0.16, 0.26$ and 0.40 from left to right) of the Q-criterion isosurfaces inside the left ventricle model.

Furthermore, the impact of tube length on flow quality was assessed by testing lengths of $L = 1D, 2D, 3D, 4D$ and $5D$, where D represents the inlet tube diameter. The tube length was identified as a critical parameter, as the incoming flow required adaptation prior to reaching the left ventricle. Testing with tube lengths H below $2D$, such as $1D$, yielded unfavorable results due to the limited adaptation space. Conversely, lengths exceeding this threshold did not markedly enhance the outcomes while escalating the computational burden of the model. Consequently, the findings suggest that a tube length of $L = 2D$ is optimal for ensuring a precise flow profile prior to its entry into the ventricle in the most efficient manner.

In conclusion, the optimal configuration for our simulations incorporates a velocity or mass flow inlet with a temporal profile based on reference data, employs a hyperbolic tangent spatial distribution for idealized geometries (or a plug profile for patient-specific cases), and uses an inlet tube length of at least $2D$. This combination has proven to be the most efficient in capturing the vortical features within the LV model.

2.4.3. Outlet

In order to simplify our model, we matched the tube length at the outlet to that of the inlet. This decision was based on the understanding that the outlet length has minimal impact on the results, as it is mainly

associated with the outflow and does not directly affect the formation of the vortex ring.

The primary consideration at the outlet is the selection between a free pressure outlet and a mass flow outlet with a controlled time profile. A free pressure outlet would necessitate the implementation of a mechanism to simulate the periodic opening and closing of the aortic valve. One potential approach would be to temporarily convert the boundary to a wall during diastole (when the heart relaxes) and then switch back to a pressure outlet during systole (when the heart contracts). However, our experimental findings have indicated that this methodology can potentially introduce noise and instability immediately following these transitions. Nevertheless, these disturbances tend to stabilize after a few time steps.

An alternative option was considered, namely the utilization of a mass flow outlet. This approach facilitates the modeling of aortic valve closure by enabling the flow to be set to zero during diastole without modifying the boundary conditions. Furthermore, the mass flow outlet offers enhanced control over the flow during systole, enabling precise matching of the flow rate to the volume changes in the left ventricle (LV), which helps prevent numerical instabilities.

In conclusion, the findings of our study indicate that a mass flow outlet represents the optimal choice for controlling outflow dynamics in LV simulations. This is due to the fact that it permits straightforward programming of zero outflow during diastole and facilitates more precise control of the flow rate during systole, thereby reducing the likelihood of errors.

2.5. Numerical schemes

The simulation is transient, and thus an implicit time-stepping scheme was employed to ensure numerical stability while allowing for larger time steps than would be possible with explicit methods. The temporal discretization was of second order, thereby ensuring enhanced accuracy in resolving time-dependent phenomena. Gradient calculations were performed using the least-squares approach, which offers a precise representation of flow field variations on the unstructured mesh. To discretize the advection terms, the Second-Order Upwind scheme was employed, selected for its enhanced accuracy in capturing flow gradients and minimal numerical diffusion. In order to couple pressure and velocity, the Pressure-Implicit with Splitting of Operators (PISO) formulation was employed, which has been demonstrated to be particularly effective for transient simulations, offering improved convergence and stability. The time step size was set to $\delta t = 5 \cdot 10^{-4}$ seconds, with 50 internal iterations per time step to ensure convergence at each timestep. The Courant-Friedrichs-Lewy (CFL) number was adapted to the specific details of the flow to maintain stability and accuracy. The wall treatment used is Implicit Tree, as it provided sufficient robustness for the simulation setup.

3. Validation

To ensure the accuracy and efficiency of our simulation results, in Ref. [16] we showed the validation of our findings using two different CFD solvers implementations: Ansys Fluent [15] and Star-CCM+ [8]. For the sake of clarity, we provide a summary of the validation and implementation differences. Moreover, this article also introduces the capability of the present setup to properly follow the temporal evolution of the vortex ring compared to literature.

The boundary conditions used for both commercial solver implementations were identical: velocity inlet and mass flow outlet, with the temporal profile extracted from the flow rate chart (see Fig. 4). The movement of the wall was extracted from the integration of the aforementioned graph for both solvers, but the method of introduction differs for each solver as previously stated in Sec. 2.4.1. In the case of Star-CCM+, the incremental evolution of the volume is introduced together with the maximum displacement of each point. In contrast, for Fluent, it

is necessary to introduce each time instant of the mesh in order to move the wall to the desired location at each time step. Moreover, the automatic meshing algorithms employed during the meshing process result in disparate outcomes despite the utilization of identical parameter values in both solvers. Additionally, the wall movement, and consequently, the volumetric mesh element movement, is executed in a manner that differs between solvers. Finally, the way of solving the flow equations is also specific to each solver. These specificities may also contribute to any difference observed.

We evaluated the convergence of our simulations using three different mesh sizes in both Fluent and Star-CCM+. These included coarse (0.3 million elements for both), medium (1 million and 0.9 million elements), and fine (1.6 million and 1.2 million elements) meshes, respectively. Our primary metric for validation was the total kinetic energy (TKE) within the ventricular cavity, excluding the inlet and outlet tubes, averaged over four cardiac cycles. This metric is shown in Fig. 6 for both commercial solvers. The results exhibit a consistent pattern with minor fluctuations in peak values, with a relative root mean square error between the finest grids of less than 7%.

Moreover, for each solver individually, we observed that the TKE distributions converged to consistent profiles when refining the mesh. This convergence can also be seen in Table 2 where we display the relative error between the current mesh size and the finest. For medium meshes the error is around 1% for both solvers, indicating that our simulations are reliable and accurate.

Recall that this work focuses on the formation and evolution of the vortex ring, a topic that has been extensively examined in the existing literature (for further details, please see Ref. [32]). Fig. 7 illustrates this process, showing the results for Star-CCM+ on the top row and the same isosurfaces for the Ansys Fluent solver on the bottom row for four different time instants during diastole. Firstly, in the initial phase of diastole (at time point $t^* = 0.16$), the vortex ring is formed at the exit of the inlet tube, which represents the mitral valve, when it opens during the E-wave. In the initial phase, the vortex ring assumes a circular configuration. As it progresses through the ventricle, at time $t^* = 0.26$, the ring exhibits a tilting motion, influenced by the proximity of the wall of one of its sides and the accompanying reduction in inflow velocity. At time $t^* = 0.40$, interactions between the vortex ring and the ventricular walls result in the formation of secondary vortex tubes, which generate complex instabilities. These instabilities tend to grow, and by the time of the latter diastole ($t^* = 0.56$), they have caused the vortex ring to dissipate. In its place, a second, smaller vortex ring has appeared in the mitral valve due to the A-wave. It is noteworthy that the results presented in Fig. 7 obtained with both solvers are in close agreement with each other and with the documented results in Ref. [17] Fig. 3.

By validating our simulations using two different CFD solver implementations, we have demonstrated the robustness and accuracy of our approach in capturing critical hemodynamic features, such as the vortex ring, which strengthens the reliability of our findings. Furthermore, we have provided a highly detailed explanation of all critical aspects of the CFD simulation setup compared to other studies in the literature. This includes geometry construction, flow modeling, wall motion, and implementation of inlet and outlet conditions. Our decisions and results are thoroughly supported by references. In addition, this article is complemented by an online tutorial available on our website [14], which facilitates the reproduction of consistent results.

4. Conclusions

This study has highlighted the significant influence of simulation conditions on the fidelity and efficiency of modeling intraventricular cardiac flows. We have discussed that the choice of geometry, whether idealized or patient-specific, has a profound impact on both the computational complexity and the physiological accuracy of the simulations. While patient-specific models could provide detailed insights, they require higher computational resources and sophisticated data interpola-

Table 2
The number of elements and the relative error for each solver and mesh employed.

Mesh size	Ansys fluent		Star-CCM+	
	N° elements	Relative error (%)	N° elements	Relative error (%)
Coarse	0.3 M	7.80	0.3 M	7.37
Medium	1.0 M	1.02	0.9 M	0.91
Fine	1.6 M	-	1.2 M	-

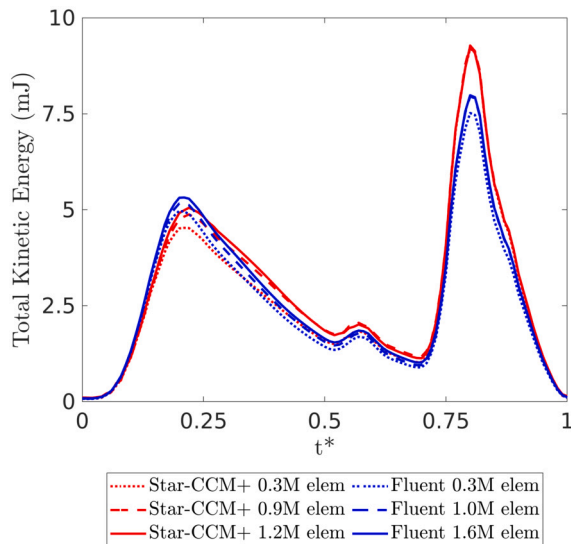


Fig. 6. Comparison of the total kinetic energy evolution over a heart cycle, averaged across four cycles, for Fluent (blue) and STAR-CCM+ (red) simulations. Results are shown for coarse (dotted line), medium (dashed line), and fine (solid line) mesh resolutions.

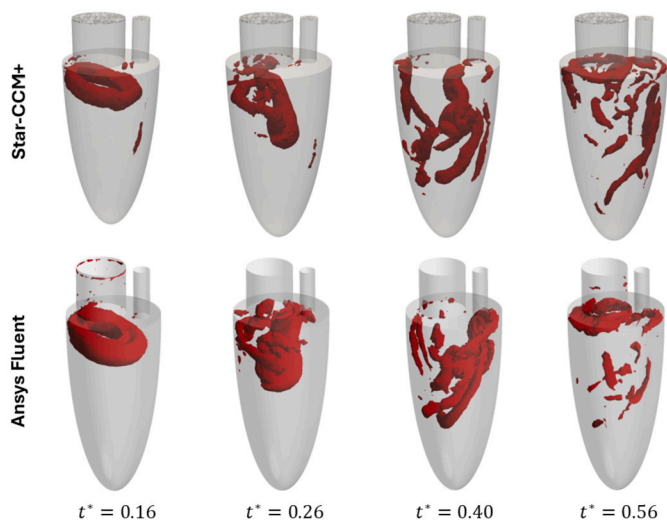


Fig. 7. Isocontours of the Q-Criterion inside the ventricular cavity that show the evolution of the vortex ring for both solvers during diastole.

tion methods. Conversely, idealized geometries, although less detailed, provide sufficient accuracy to capture critical flow features such as the vortex ring at reduced computational effort.

Our investigations into the flow conditions confirmed that the assumption of laminar flow is sufficient to simulate cardiac dynamics at the scale of the LV model, thus avoiding the additional complexity of turbulence models. The boundary conditions, in particular the dynamic modeling of wall motion and the careful choice of the inflow and outflow conditions, were crucial for accurately capturing the essential features

of cardiac flow. The implementation of a moving wall boundary, as opposed to a static wall, proved to be an effective method for enhancing the capability of our study to reproduce key physiological behaviors, including vortex ring formation and flow recirculation.

Furthermore, our results underscore the need to employ a refined mesh near the walls to resolve small-scale phenomena and dynamically adapt to wall motion, thereby improving the overall quality of the simulation.

Validation of our simulations through comparisons with commercial solvers Ansys Fluent and Star-CCM+ confirmed the reliability and robustness of our approach. Both solver implementations showed comparable patterns in total kinetic energy and vortex ring formation and evolution, closely matching each other and the existing literature. This double validation reinforces the accuracy of our methodology and its applicability in realistic cardiac flow simulations.

A more detailed examination of the flow dynamics, particularly the vortex ring dynamics, has revealed that simulations conducted with an idealized LV model are capable of accurately capturing the formation of the vortex ring at the onset of diastole and its subsequent evolution throughout the cardiac cycle. During this process, the vortex ring manifests as a circular ring due to the inflow from the mitral valve. As a consequence of the influence of the closest wall, the flow tilts, thereby fostering the growth of instability. This results in the dissipation of the vortex ring just prior to the onset of systole, which aligns with the pumping of blood out of the heart.

In conclusion, this study provides a comprehensive assessment of the critical conditions needed to accurately and efficiently simulate the complex dynamics within the LV model, providing insights that could be instrumental in advancing the field of cardiovascular research and the development of diagnostic and therapeutic strategies.

CRedit authorship contribution statement

E. Lazpita: Writing – review & editing, Writing – original draft, Visualization, Validation, Software, Resources, Methodology, Formal analysis. **A. Mares:** Writing – review & editing, Validation, Software, Resources. **P. Quintero:** Writing – review & editing, Validation, Software, Resources. **J. Garicano-Mena:** Writing – review & editing, Writing – original draft, Validation, Supervision, Project administration, Methodology. **S. Le Clairche:** Writing – review & editing, Writing – original draft, Validation, Supervision, Project administration, Methodology.

Declaration of competing interest

The authors declare that they have no known competing financial interests or personal relationships that could have appeared to influence the work reported in this paper.

Acknowledgements

The authors acknowledge the grants TED2021-129774B-C21 and PLEC2022-009235 funded by MCIN/AEI/10.13039/501100011033 and by the European Union “NextGenerationEU”/PRTR and the grant PID2023-147790OB-I00 funded by MCIU/AEI/10.13039/501100011033/FEDER, UE. The authors gratefully acknowledge the Universidad Politécnica de Madrid (www.upm.es) for providing computing resources on Magerit Supercomputer. P.Q. would like to acknowledge the support of DIDIMO, Grant PLEC2021-007614 funded

by MCIN/AEI/10.13039/501100011033 and, as appropriate, by the “ERDF A way of making Europe”, and the “European Union NextGenerationEU/PRTR”.

This work has been fueled by lively discussions with Prof. M. Neidling from Institute of Applied Medical Engineering - RWTH Aachen, and with our colleagues E. Lara y M. Villalba-Orero in the *Centro Nacional de Investigaciones Cardiovasculares* (CNIC). The authors thankfully acknowledge the computer resources, technical expertise, and assistance provided by Prof. M. Chávez and Prof. E. Valero from Universidad Politécnica de Madrid.

Data availability

I have shared the link to the data in Attach Files, and also as a citation in the manuscript.

[Simulation Codes \(Original data\)](#) (GitHub Website)

References

- [1] P. Dorairaj, A. Shuchi, T.A. Gaziano, J.C. Mbanya, Y. Wu, R. Nugent, Disease Control Priorities: Volume 5. Cardiovascular, Respiratory, and Related Disorders, 3rd ed., 2017, <https://openknowledge.worldbank.org/handle/10986/28875>.
- [2] P.C. Africa, I. Fumagalli, M. Bucelli, A. Zingaro, M. Fedele, A. Quarteroni, lifex-cfd: an open-source computational fluid dynamics solver for cardiovascular applications, *Comput. Phys. Commun.* 296 (2024) 109039, <https://doi.org/10.48550/arXiv.2304.12032>.
- [3] T.B. Baturalp, S. Borkurt, Design and analysis of a polymeric left ventricular simulator via computational modelling, *Biomimetics* 9 (5) (2024) 269, <https://doi.org/10.3390/biomimetics9050269>.
- [4] M. Topalović, Aleksandar Bodić, Miloš S. Pešić, Miljan S. Milošević, M. Miroslav Živković, Numerical simulations of blood flow through left ventricle using sph and fvm methods – a comparative study, *J. Serb. Soc. Comput. Mech.* 17 (2) (2023), <https://doi.org/10.24874/jsscm.2023.17.02.02>.
- [5] A. Zingaro, I. Fumagalli, L. Dede, M. Fedele, P.C. Africa, A.F. Corno, A. Quarteroni, A geometric multiscale model for the numerical simulation of blood flow in the human left heart, *arXiv:2110.02114*, 2021.
- [6] L. Goubergrits, K. Vellguth, L. Obermeier, A. Schlieff, L. Tautz, J. Bruening, H. Lamecker, A. Szengel, O. Nemchyna, C. Knosalla, T. Kuehne, CT-based analysis of left ventricular hemodynamics using statistical shape modeling and computational fluid dynamics, *Front. Cardiovasc. Med.* 9 (2022) 901902, <https://doi.org/10.3389/fcvm.2022.901902>.
- [7] J.N. Thiel, D. Verhülsdonk, U. Steinseifer, K. Linden, U. Herberg, I. Friehs, D. Diaz-Gil, M. Neidling, An interactive computational pipeline to investigate ventricular hemodynamics with real-time three-dimensional echocardiography and computational fluid dynamics, *Eng. Rep.* (2024) e13041, <https://doi.org/10.1002/eng2.13041>.
- [8] Siemens Industries Digital Software, *Simcenter STAR-CCM+, version 2023.06*, Siemens, 2023.
- [9] S. Mohammad, P. Majumdar, Computational fluid dynamics analysis of blood flow through stented arteries, in: *ASME International Mechanical Engineering Congress and Exposition*, vol. 56215, 2013, V03AT03A047.
- [10] T. Schenkel, M. Malve, M. Reik, M. Markl, B. Jung, H. Oertel, MRI-based CFD analysis of flow in a human left ventricle: methodology and application to a healthy heart, *Ann. Biomed. Eng.* 37 (2009) 503–515, <https://doi.org/10.1007/s10439-008-9627-4>.
- [11] V.T. Nguyen, S.N. Wibowo, Y.A. Leow, H.H. Nguyen, Z. Liang, H.L. Leo, A patient-specific computational fluid dynamic model for hemodynamic analysis of left ventricle diastolic dysfunctions, *Cardiovasc. Eng. Technol.* 6 (2015) 412–429, <https://doi.org/10.1007/s13239-015-0244-8>.
- [12] J.O. Mangual, E. Kraigher-Krainer, A. De Luca, L. Toncelli, A. Shah, S. Solomon, G. Galanti, F. Domenichini, G. Pedrizzetti, Comparative numerical study on left ventricular fluid dynamics after dilated cardiomyopathy, *J. Biomech.* 46 (10) (2013) 1611–1617, <https://doi.org/10.1016/j.jbiomech.2013.04.012>.
- [13] A. Riva, S. Saitta, F. Sturla, G. Disabato, L. Tondi, A. Camporeale, D. Giese, S. Castelvécchio, L. Menicanti, A. Redaelli, M. Lombardi, E. Votta, Left ventricle diastolic vortex ring characterization in ischemic cardiomyopathy: insight into atrio-ventricular interplay, *J. Cardiovasc. Magn. Reson.* 26 (2024), <https://doi.org/10.1016/j.jocmr.2024.100362>.
- [14] DigitHEART, New tools and models for predicting heart disease progression and treatment response, *ModelFlows-cardiac*, <https://modelflows.github.io/modelflowsapp/cardiacpathologydetection/>.
- [15] Ansys Fluent Academic Research, Release 2023 R1, Help System, Ansys Fluent Theory Guide, Ansys, Inc.
- [16] E. Lazpita, M. Nagargoje, S. Clainche, J. Garicano-Mena, On the numerical simulation of left ventricle models, in: *ECCOMAS 2024*, https://www.scipedia.com/public/Lazpita_et_al_2024a.
- [17] X. Zheng, J.H. Seo, V. Vedula, T. Abraham, R. Mittal, Computational modeling and analysis of intracardiac flows in simple models of the left ventricle, *Eur. J. Mech. B, Fluids* 35 (2012) 31–39, <https://doi.org/10.1016/j.euromechflu.2012.03.002>.
- [18] V. Vedula, S. Fortini, J.H. Seo, G. Querzoli, R. Mittal, Computational modeling and validation of intraventricular flow in a simple model of the left ventricle, *Theor. Comput. Fluid Dyn.* 28 (2014) 589–604, <https://doi.org/10.1007/s00162-014-0335-4>.
- [19] F. Kong, S.C. Shadden, Whole heart mesh generation for image-based computational simulations by learning free-form deformations, in: *International Conference on Medical Image Computing and Computer-Assisted Intervention*, Springer International Publishing, Cham, 2021, pp. 550–559.
- [20] Centro nacional de investigaciones cardiovasculares (CNIC), <https://www.cnic.es/es>.
- [21] D. Collià, G. Libero, G. Pedrizzetti, V. Ciriello, Surrogate models provide new insights on metrics based on blood flow for the assessment of left ventricular function, *Sci. Rep.* 12 (1) (2022) 8695, <https://doi.org/10.1038/s41598-022-12560-3>.
- [22] V. Meschini, R. Mittal, R. Verzico, Systolic anterior motion in hypertrophic cardiomyopathy: a fluid–structure interaction computational model, *Theor. Comput. Fluid Dyn.* 35 (2021) 381–396, <https://doi.org/10.1007/s00162-021-00564-0>.
- [23] J.P. Simpson, J.H. Leyle, The influence of Womersley number on non-Newtonian effects: transient computational study of blood rheology, *J. Fluids Eng.* 145 (1) (2023) 011206, <https://doi.org/10.1115/1.4055400>.
- [24] G. He, L. Han, J. Zhang, A. Shah, D.J. Kaczorowski, B.P. Griffith, Z. Wu, Numerical study of the effect of LVAD inflow cannula positioning on thrombosis risk, *Comput. Methods Biomech. Biomed. Eng.* 25 (8) (2022) 852–860, <https://doi.org/10.1080/10255842.2021.1984433>.
- [25] A. Tagliabue, L. Dede, A. Quarteroni, Complex blood flow patterns in an idealized left ventricle: a numerical study, *Chaos* 27 (9) (2017), <https://doi.org/10.1063/1.5002120>.
- [26] M. Bucelli, A. Zingaro, P.C. Africa, I. Fumagalli, L. Dede, A. Quarteroni, A mathematical model that integrates cardiac electrophysiology, mechanics, and fluid dynamics: application to the human left heart, *Int. J. Numer. Methods Biomed.* 39 (3) (2023) e3678, <https://doi.org/10.1002/cnm.3678>.
- [27] J. Korte, T. Rauwolf, J.N. Thiel, A. Mitrash, P. Groschopp, M. Neidling, A. Schmeißer, R. Braun-Dullaes, P. Berg, Hemodynamic assessment of the pathological left ventricle function under rest and exercise conditions, *Fluids* 8 (2) (2023) 71, <https://doi.org/10.3390/fluids8020071>.
- [28] F. Tajeddini, D.A. Romero, D. McClarty, J. Chung, C.H. Amon, Workflow comparison for combined 4d mri/cfd patient-specific cardiovascular flow simulations of the thoracic aorta, *J. Fluids Eng.* 145 (6) (2023) 061106, <https://doi.org/10.1115/1.4057047>.
- [29] S. Wang, X. Li, R. Zhang, Z. Sha, Z. Wu, Q. Zhang, Thermal distribution characteristics related to the transformer fine structure predicted by CFD-based spline interpolation, *IEEE Trans. Dielectr. Electr. Insul.* 30 (2) (2022) 892–901, <https://doi.org/10.1109/TDEI.2022.3233340>.
- [30] X. Liu, C. Liu, C. Chen, H. Kui, Longitudinal stability analysis of underwater towed body based on CFD, *J. Phys. Conf. Ser.* 2441 (1) (2023, March) 012041, <https://iopscience.iop.org/article/10.1088/1742-6596/2441/1/012041/meta>.
- [31] The MathWorks, Inc., MATLAB version: 9.13.0 (R2022b), Available: <https://www.mathworks.com>, 2022.
- [32] T.B. Le, F. Sotiropoulos, D. Coffey, D. Keefe, Vortex formation and instability in the left ventricle, *Phys. Fluids* 24 (9) (2012), <https://doi.org/10.1063/1.4747164>.